Contact interaction model for the η and η' mesons in a Schwinger-Dyson-Bethe-Salpeter approach to QCD: Masses, decay widths, and transition form factors

Bilgai Almeida Zamora[1], Enrique Carreon Martínez[2], Jorge Segovia,[3] and J. J. Cobos-Martínez[4,*]

[1]*Departamento de Investigación en Física, Universidad de Sonora, Boulevard Luis Encinas J. y Rosales, Colonia Centro, Hermosillo, Sonora 83000, México*
[2]*Departamento de Física, Centro de Investigación y de Estudios Avanzados del Instituto Politécnico Nacional, Apartado Postal 14-740, 07000, Ciudad de México, México*
[3]*Departamento de Sistemas Físicos, Químicos y Naturales, Universidad Pablo de Olavide, E-41013, Sevilla, Spain*
[4]*Departamento de Física, Universidad de Sonora, Boulevard Luis Encinas J. y Rosales, Colonia Centro, Hermosillo, Sonora 83000, México*

We construct a contact interaction model for the η and η' mesons in the SDE-BSE approach to QCD and compute several static properties of these mesons and their transition form factors. We find that this model gives an excellent description of the η and η' static properties, namely, their masses, decay width, and decay constants. However, a contact interaction disagrees with experimental data for Q^2 greater than 2 GeV^2, and produces transition form factors in conflict with perturbative QCD prediction. This is not surprising and the reasons for this are explained.

I. INTRODUCTION

Quantum chromodynamics (QCD), the theory of quarks, gluons, and their interactions, is the accepted theory of the strong interactions at the fundamental level. Although QCD dictates the dynamics of quarks and gluons, and therefore, in principle, the strucure and dynamics of hadrons, which are bound states of quarks and gluons, the nonperturbative nature of QCD makes this a difficult problem. In the low energy, nonperturbative regime of QCD, the emergent phenomena of chiral symmetry breaking and confinement govern the static and dynamic properties of hadrons; for example, these are responsible for 99% of the mass of the visible universe; see, for example, Refs. [1,2] and references therein.

Within the framework of Schwinger-Dyson (SDE) and Bethe-Salpeter equations (BSE) of QCD, we can investigate the structure and dynamics of hadrons through first principles in the continuum. However, drawing a connection between QCD and hadron observables, through the SDE-BSE system, is a difficult task due to the infinite number of equations we need to confront—and that is why modeling remains a keystone in hadron physics. Despite this difficulty, great progress has been made for more than three decades using the SDE-BSE approach to nonperturbative QCD and hadron physics, and this has become a powerful and reliable tool to investigate strong interaction phenomena; see, for example, Refs. [3–6]. SDE and BSEs for QCD have been extensively applied to the study of hadrons in vacuum and at finite density and temperature in a variety of truncation schemes and degrees of sophistication; see Ref. [6] for a recent review.

More than a decade ago a simple alternative within the SDE-BSE approach was proposed, initially to study pion properties, assuming that quarks interact not via massless vector-boson exchange but instead through a symmetry preserving vector-vector contact interaction (CI) [7,8]. Over the ensuing years, this contact interaction has been used to investigate static and dynamic properties of hadrons in vacuum, such as masses, decay constants, electromagnetic elastic and transition form factors, parton distribution functions, and generalized parton distribution functions [7–31] and at finite temperature and density to study, for example, the phase diagram of QCD [32–34].

The results obtained from the contact interaction model are quantitatively comparable to those obtained using sophisticated QCD model interactions. Furthermore, the weaknesses and strengths of this interaction have been

*Corresponding author.
jesus.cobos@unison.mx

identified and understood. Despite its weaknesses, the contact interaction has emerged as a powerful tool in the investigation of hadron properties. We take this as a sufficient justification to employ this interaction in order to construct a contact interaction model for the η and η' mesons in the SDE-BSE approach to QCD and compute several static properties of these mesons and their transition form factors. We will find that this model gives an excellent description of the η and η' static properties and this makes it an excellent tool for the investigation of $U_A(1)$ symmetry restoration at finite temperature and density in the SDE-BSE approach to QCD. This will be reported elsewhere.

This article is organized as follows. In Sec. II, we briefly present the Schwinger-Dyson and Bethe-Salpeter equations of QCD in rainbow-ladder truncation with a contact interaction. The model parameters for this piece of the interaction are fixed by pion and kaon static properties. In Sec. III, we extend the rainbow-ladder truncation to include a phenomenological kernel that represents the non-Abelian anomaly. The model parameters for this part of the interaction are fitted by the masses and decay widths of the η and η' mesons. In Sec. IV, we compute the η and η' transition form factors using the constructed contact interaction model. Finally, in Sec. V we give a summary and conclusions.

II. SDE-BSE FORMALISM

In this section we briefly introduce the SDE-BSE formalism of QCD. Our focus will be on the contact interaction since this is employed to produce the results reported in this article. See Refs. [3–6] for comprenhensive reviews on the SDE-BSE approach to QCD and hadron physics.

A. The quark SDE and the contact interaction

The f-flavor dressed-quark propagator S_f is obtained by solving the quark SDE

$$S_f^{-1}(p) = i\gamma \cdot p + m_f + \Sigma_f(p), \tag{1}$$

$$\Sigma_f(p) = \int \frac{\mathrm{d}^4 q}{(2\pi)^4} g^2 D_{\mu\nu}(p-q) \frac{\lambda^a}{2} \gamma_\mu S_f(q) \Gamma_\nu^a(p,q), \tag{2}$$

where g is the strong coupling constant, $D_{\mu\nu}$ is the dressed gluon propagator, Γ_ν^a is the dressed quark-gluon vertex, m_f is the f-flavor current-quark mass, and λ^a are the usual Gell-Mann matrices. The chiral limit is defined by $m_f = 0$.

The SDEs constitute an infinite set of coupled nonlinear integral equations and thus a tractable problem is defined once a truncation scheme has been specified. In practice, this is achieved by specifying the gluon propagator and the quark-gluon vertex.

There is extensive literature [7–31] where it has been shown that the static properties of low-lying mesons and baryons can be described by assuming that the quarks

interact, not via massless vector-boson exchange, but instead through a symmetry preserving vector-vector contact interaction (CI) with a finite gluon mass

$$g^2 D_{\mu\nu}(k) = \delta_{\mu\nu} \frac{4\pi\alpha_{\mathrm{IR}}}{m_g^2} \equiv \alpha_{\mathrm{eff}} \delta_{\mu\nu}, \tag{3}$$

$$\Gamma_\mu^a(p,q) = \frac{\lambda^a}{2} \gamma_\mu, \tag{4}$$

where $m_g \sim 500$ MeV is an infrared gluon mass scale which is generated dynamically in QCD [35–40], and α_{IR} is specified by the strength of the infrared interaction in QCD. There is a critical value of α_{eff} above which chiral symmetry is dynamically broken.

Equations (3) and (4) specify the so-called rainbow truncation of the quark SDE within a contact interaction. This truncation scheme generates a momentum independent dymamical mass M_f for the dressed-quark propagator [7,8]

$$S_f^{-1}(p) = i\gamma \cdot p + M_f. \tag{5}$$

The dynamical, flavor-dependent, constant mass M_f is obtained by solving

$$M_f = m_f + \frac{\alpha_{\mathrm{eff}} M_f}{3\pi^2} \int_0^\infty \mathrm{d}q^2 \frac{q^2}{q^2 + M_f^2}. \tag{6}$$

Since the integral in Eq. (6) is divergent, we must specify a regularization prescription. We use the proper time regularization scheme to write $(q^2 + M_f^2)^{-1}$ in Eq. (6) as

$$\begin{aligned}
\frac{1}{q^2 + M_f^2} &= \int_0^\infty d\tau \mathrm{e}^{-\tau(q^2 + M_f^2)} \\
&\rightarrow \int_{\tau_{\mathrm{UV}}}^{\tau_{\mathrm{IR}}} d\tau \mathrm{e}^{-\tau(q^2 + M_f^2)} \\
&= \frac{\mathrm{e}^{-\tau_{\mathrm{UV}}(q^2 + M_f^2)} - \mathrm{e}^{-\tau_{\mathrm{IR}}(q^2 + M_f^2)}}{q^2 + M_f^2}.
\end{aligned} \tag{7}$$

In Eq. (7), $\tau_{\mathrm{IR}}^{-1} \equiv \Lambda_{\mathrm{IR}}^2$ and $\tau_{\mathrm{UV}}^{-1} \equiv \Lambda_{\mathrm{UV}}^2$ are infrared and ultraviolet regulators, respectively, which will be specified later. A nonzero value for τ_{IR} implements confinement by ensuring the absence of quarks production thresholds [41]. It has been shown that an excitation described by a poleless propagator would never reach its mass shell [41]. Moreover, since the CI is not renormalizable, Λ_{UV} cannot be removed, but instead plays a dynamical role and sets the scale for all dimensioned physical quantities. After integration over q^2, Eq. (6) can be written as

$$M_f = m_f + \frac{\alpha_{\mathrm{eff}} M_f}{3\pi^2} \int_{\tau_{\mathrm{UV}}}^{\tau_{\mathrm{IR}}} \mathrm{d}\tau \tau^{-2} \mathrm{e}^{-\tau M_f^2}. \tag{8}$$

By solving Eq. (8) we can obtain the dynamical mass of the quark of flavor f.

B. The BSE and the contact interaction

In quantum field theory, meson bound states in a given J^{PC} channel, whose flavor structure is given by a non-perturbative dressed quark-antiquark pair $(f\bar{g})$, are described by the Bethe-Salpeter equation (BSE) [42–45]

$$[\Gamma_H(p;P)]_{tu} = \int \frac{d^4q}{(2\pi)^4} [K(p,q;P)]_{tu}^{rs} [\chi(q;P)]_{sr}, \quad (9)$$

where $\chi(q;P) = S_f(q_+)\Gamma_H(q;P)S_g(q_-)$; $q_+ = q + \eta P$, $q_- = q - (1-\eta)P$; $\eta \in [0,1]$ is a momentum-sharing parameter, p (P) is the relative (total) momentum of the quark-antiquark system, with $P^2 = -m_H^2$ and m_H the mass of the meson; $S_{f(g)}$ is the nonperturbative $f(g)$-flavor dressed-quark propagator, already discussed; $\Gamma_H(p;P)$ is the meson Bethe-Salpeter amplitude (BSA), where H specifies the quantum numbers and flavor content of the meson; r, s, t, and u represent color, flavor, and spinor indices; and $K(p,q;P)$ is the quark-antiquark scattering kernel.

Equations (3) and (4) define the kernel of the quark SDE. But they also define the kernel of the BSE, Eq. (9), through the axial-vector Ward-Takahashi identity (axWTI) [46]

$$-iP_\mu\Gamma_{5\mu}(k;P) = S^{-1}(k_+)\gamma_5 + \gamma_5 S^{-1}(k_-). \quad (10)$$

This identity, which encodes the phenomenological features of dynamical chiral symmetry breaking in QCD, relates the axial-vector vertex, $\Gamma_{5\mu}(k;P)$, to the quark propagator, $S(k)$, which in turn implies a relationship between the kernel in the BSE, Eq. (9), and that in the quark SDE, Eq. (1). This relation must be preserved by any viable truncation scheme of the SDE-BSE coupled system, thus constraining the content of the quark-antiquark scattering kernel $K(p,q;P)$. For the CI, Eq. (10) implies that the quark-antiquark scattering kernel $K(p,q;P)$ is given by

$$[K_L(p,q;P)]_{tu}^{rs} = -g^2 D_{\mu\nu}(p-q)\left[\frac{\lambda^a}{2}\gamma_\mu\right]_{ts}\left[\frac{\lambda^a}{2}\gamma_\nu\right]_{ru}, \quad (11)$$

where $g^2 D_{\mu\nu}(k)$ is given by Eq. (3).

Thus, the homogeneous BSE (we use $\eta = 1$ in this work), in rainbow-ladder (RL) truncation, with a contact interaction, takes the simple form

$$\Gamma_H(p;P) = -\frac{4}{3}\alpha_{\text{eff}} \int \frac{d^4q}{(2\pi)^4} \gamma_\mu S_f(q_+)\Gamma_H(q;P)S_g(q_-)\gamma_\mu. \quad (12)$$

We note that some of the integrals that appear in Eq. (12) are also divergent but will be regulated using the proper

time regularization scheme, Eq. (7), as we will do with all divergent integrals in this work.

Since the kernel of Eq. (11) in RL truncation with a contact interaction does not depend on the external relative momentum, a symmetry-preserving regularization will give solutions which are also independent of it. Therefore, for example, the general form of the BSA for a pseudoscalar meson is given by

$$\Gamma_{\text{Ps}}(P) = \gamma_5\left[iE_{\text{Ps}}(P) + \frac{1}{2M_R}\gamma \cdot PF_{\text{Ps}}(P)\right], \quad (13)$$

where $M_R = M_f M_g/(M_f + M_g)$. We are interested only in pseudoscalar mesons but similar expressions to Eq. (13) can be written down for other channels.

The BSE is a homogeneous equation and thus the BSA has to be normalized by a separate condition. In the RL approximation, the normalization condition is [42–45]

$$1 = N_c \frac{\partial}{\partial P^2} \int \frac{d^4q}{(2\pi)^4} \text{Tr}[\bar{\Gamma}_H(-Q)S(q_+)\Gamma_H(Q)S(q_-)]|_{Q=P}, \quad (14)$$

where $P^2 = -m_H^2$, Γ_H is the normalized BSA of the meson H, and $\bar{\Gamma}_H$ is its charge-conjugated version.

Once the BSA has been canonically normalized, we can compute observables with it. For example, the leptonic decay constant of a pseudoscalar meson, f_{Ps}, can be calculated from

$$P_\mu f_{\text{Ps}} = N_c \int \frac{d^4q}{(2\pi)^4} \text{Tr}[\gamma_5\gamma_\mu S_f(q_+)\Gamma_{\text{Ps}}(P)S_g(q_-)], \quad (15)$$

where the trace is over Dirac indices.

C. Numerical results with the RL contact interaction

We work in the isospin symmetric limit, where $m_u = m_d$ and use the notation $m_l \equiv m_u$ for the current mass of the light quarks. The model parameters in the RL truncation are thus m_l, the strange current quark mass m_s, the effective coupling α_{eff} (or α_{IR} since m_g is fixed to 500 MeV), and the ultraviolet regulator Λ_{UV}. The infrared regulator Λ_{IR} is fixed to approximately $\Lambda_{\text{QCD}} = 240$ GeV. The three parameters m_l, α_{eff} (or α_{IR}), and Λ_{UV} were fixed in Ref. [7] from the pion mass, pion decay constant, and chiral condensate using a least-squares procedure. We use a normalization of the BSA amplitude such that the experimental pion decay constant is $f_\pi = 93$ MeV. Reference [7] gives $m_l = 8$ MeV, $\alpha_{\text{eff}} = 1/(110 \text{ MeV})^2 = 8.3 \times 10^{-5}$ MeV^{-2} (this gives $\alpha_{\text{IR}} = 0.52\pi$ for $m_g = 500$ MeV), and $\Lambda_{\text{UV}} = 823$ MeV.

In order to determine the current mass of the strange quark, we fit experimental values of kaon mass, $m_K = 497$ MeV. This gives $m_s = 187$ MeV, and we predict the value $f_K = 96$ MeV for the kaon decay constant. The value obtained

TABLE I. Results for pion and kaon static properties (in MeV) obtained with $m_l = 8\,\text{MeV}$, $m_s = 187\,\text{MeV}$, $\alpha_{\text{eff}} = 1/(110\,\text{MeV})^2 = 0.91 \times 10^{-4}\,\text{MeV}^{-2}$, and $\Lambda_{\text{UV}} = 823$ MeV. The dynamical masses for the light and strange quarks are $M_l = 410$ MeV, $M_s = 557$ MeV, respectively. The values in the second row are taken from the Particle Data Group [48].

	m_π	m_K	f_π	f_K
PDG [48]	140	497	93	110
RL-CI	141	500	94	96

here for f_K is similar to the one obtained in the NJL model of QCD, where it is found that $f_K = 91$ MeV [47]. Recent experimental analyses of the current quark masses and pseudoscalar meson leptonic decay constants have found $m_s/m_l = 27.33^{+0.67}_{-0.77}$ and $f_K/f_\pi = 1.193(2)$ [48]. Our results for these ratios are $m_s/m_l = 23.375$ and $f_K/f_\pi = 1.03$, which reasonably agree with the experimental values. In Table I we give a summary of the values for the CI-RL model parameters.

III. INCLUDING THE NON-ABELIAN ANOMALY

The RL kernel is insufficient to describe the η and η' properties, since, for example, it does not produce mixing between $u\bar{u}$, $d\bar{d}$, and $s\bar{s}$ correlations. A way to introduce mixing between these correlations, and therefore improve the description of the η and η' mesons, is to go beyond the RL truncation and add to K_L, given in Eq. (11), a term that represents the non-Abelian anomaly; that is

$$K(p, q; P) = K_{\text{L}}(p, q; P) + K_A(p, q; P), \quad (16)$$

where [49]

$$[K_A(p, q; P)]^{rs}_{tu} = \xi(\cos^2\theta[\mathcal{Z}i\gamma_5]_{rs}[\mathcal{Z}i\gamma_5]_{tu} + \sin^2\theta[\hat{\mathcal{Z}}P\gamma_5]_{rs}[\hat{\mathcal{Z}}P\gamma_5]_{tu}) \quad (17)$$

with $\mathcal{Z} = \text{diag}(1, 1, M_l/M_s)$ and $\hat{\mathcal{Z}} = (1/M_l)\mathcal{Z}$ matrices in flavor space. Here, the dynamical masses of the light M_l and strange M_s quarks are fixed only from pion and kaon phenomenology. We note that the origin of K_A is phenomenological; see Ref. [49].

In Eq. (17), the model parameters are ξ and θ: ξ is a dimensionless coupling strength and θ controls the relative strength of the two tensor structures. In principle, ξ would also depend on the relative momenta between the quark and the antiquark; however, to be consistent with the contact interaction RL kernel, we require ξ to be a constant. Then, this gives a BSA for the η and η' independent of the relative momentum between the quark and the antiquark, which is a signature of a contact interaction. The model parameters ξ

and θ are determined from experimental values of the masses, decay constants, and decay widths of the η and η'.

A. Leptonic decay constants and two-photon widths for the η and η'

We now discuss the η and η' static properties in our contact interaction model. For this, it is convenient to work with the $N_f = 3$ quark flavor basis, where the η and η' wave functions can be written as [50–52]

$$\chi_h(p; P) = d_l\chi^l_h(p; P) + d_s\chi^s_h(p; P), \qquad h = \eta, \eta', \quad (18)$$

where $d_l = \text{diag}(1, 1, 0)$, $d_s = \text{diag}(0, 0, \sqrt{2})$ are matrices in flavor space. Here $\chi^l_h(p; P)$ and $\chi^s_h(p; P)$ are Bethe-Salpeter wave functions for the $\bar{l}l$ and $s\bar{s}$ correlations in the η and η' mesons, and the corresponding Bethe-Salpeter amplitudes are obtained from

$$\chi^f_h(p; P) = S_f(p_+)\Gamma^f_h(p; P)S_f(p_-), \quad (19)$$

where $f = l, s$. Thus, the BSA of the η and η' are given by $(h = \eta, \eta')$

$$\Gamma_h(p; P) = d_l\Gamma^l_h(p; P) + d_s\Gamma^s_h(p; P). \quad (20)$$

Inserting Eqs. (18), (19), and (20) into the Bethe-Salpeter equation, Eq. (9), we obtain a set of coupled equations for the light and strange correlations Γ^l_h and Γ^s_h in the η and η' mesons, which can be solved by matrix methods [15]:

$$\begin{aligned}
\Gamma^l_h(p; P) = &-\frac{4}{3}\int \frac{\mathrm{d}^4q}{(2\pi)^4} g^2 D_{\mu\nu}(k - q)\gamma_\mu\chi^l_h(q; P)\gamma_\nu \\
&+ \xi\int \frac{\mathrm{d}^4q}{(2\pi)^4}\cos^2\theta\,\mathrm{Tr}[Z\gamma_5\chi_h(q; P)]i\gamma_5 \\
&+ \xi\int \frac{\mathrm{d}^4q}{(2\pi)^4}\frac{\sin^2\theta}{M_l^2}\mathrm{Tr}[Z\gamma_5 P\chi_h(q; P)]\gamma_5 P,
\end{aligned} \quad (21)$$

$$\begin{aligned}
\Gamma^s_h(p; P) = &-\frac{4}{3}\int \frac{\mathrm{d}^4q}{(2\pi)^4} g^2 D_{\mu\nu}(k - q)\gamma_\mu\chi^s_h(q; P)\gamma_\nu \\
&+ \frac{\xi\nu_A}{\sqrt{2}}\int \frac{\mathrm{d}^4q}{(2\pi)^4}\cos^2\theta\,\mathrm{Tr}[Z\gamma_5\chi_h(q; P)]i\gamma_5 \\
&+ \frac{\xi\nu_A}{\sqrt{2}}\int \frac{\mathrm{d}^4q}{(2\pi)^4}\frac{\sin^2\theta}{M_l^2}\mathrm{Tr}[Z\gamma_5 P\chi_h(q; P)]\gamma_5 P,
\end{aligned} \quad (22)$$

where the trace is over flavor and Dirac indices. Indeed, these are a set of coupled equations for Γ^l_h and Γ^s_h since $\chi_h(q; P)$ $(h = \eta, \eta')$, given by Eq. (19), contains both correlations and thus produces mixing. Since the non-Abelian kernel does not introduce any dependence in the

relative momenta between the quark and the antiquark (recall that we take ξ to be independent of momenta), the BSA for the correlations Γ_h^l and Γ_h^s has the general structure

$$\Gamma_h^f(P) = \gamma_5 \left[iE_h^f(P) + \frac{1}{M_f}\not\!P F_h^f(P) \right], \qquad (23)$$

for $h = \eta, \eta'$ and $f = l, s$.

Using standard projection methods [15], Eqs. (21) and (22) can be written terms of the pseudoscalar ($E_h^{l,s}$) and pseudovector ($F_h^{l,s}$) components, which, in turn, can be written as a eigenvalue equation for the vector $(E_h^l, F_h^l, E_h^s, F_h^s)^T$ for $h = \eta, \eta'$:

$$\begin{pmatrix} E_h^l \\ F_h^l \\ E_h^s \\ F_h^s \end{pmatrix} = [K_h(P^2)]_{4\times 4} \begin{pmatrix} E_h^l \\ F_h^l \\ E_h^s \\ F_h^s \end{pmatrix}, \qquad (24)$$

where the matrix elements of $K_h(P^2)$ will be reported elsewhere. We note that the mixing between the light and strange correlations is proportional to ξ. This mixing vanishes when $\xi = 0$ and the light and strange correlations decouple, since $K_A = 0$ and K_h reduce to the RL kernel, $K_h = K_L$.

The masses of the η and η' are computed from the condition

$$\det[K_h(P^2 = m_h^2) - I_{4\times 4}] = 0. \qquad (25)$$

That is, we adjust m_h, for $h = \eta, \eta'$, until Eq. (25) is satisfied.

Since the kernel now depends on the meson momentum P, the canonical normalization condition is more complicated. For this reason, it is useful to introduce an alternative, but equivalent, normalization condition. To this end, eigenvalue $\lambda(P^2)$ is introduced on the left-hand side of Eq. (24) such that it has solutions for all P. In terms of $\lambda(P^2)$ the bound state condition now becomes

$$\lambda(P^2 = m_h^2) = 1. \qquad (26)$$

That is, we adjust m_h, for $h = \eta, \eta'$, until Eq. (26) is satisfied. The smallest mass is identified with the η mass and the largest with that of the η'.

In terms of $\lambda(P^2)$, the normalization condition for the BSA is [53,54]

$$\left[\frac{d\ln\lambda(P^2)}{dP^2} \right]_{P^2=m_h^2}^{-1} = 2\mathrm{Tr}\int \frac{d^4q}{(2\pi)^4} \left[\bar{\Gamma}_h^l(-P)\chi_h^l(q;P) \right.$$
$$\left. + \bar{\Gamma}_h^s(-P)\chi_h^s(q;P) \right], \qquad (27)$$

where trace is over color and Dirac indices.

Once the BSA has been normalized, observables such as the lepton decay constants and 2-photon decay widths can be calculated. The decay widths $h \to \gamma\gamma$ can be computed from [49]

$$\Gamma_{h\to\gamma\gamma} = \frac{9\alpha_{\mathrm{em}}^2}{64\pi^3} m_h^3 \left[c_l \frac{f_h^l}{(f^l)^2} + c_s \frac{f_h^s}{(f^s)^2} \right]^2, \qquad (28)$$

with $\alpha_{em} = 1/137$, $c_l = 5/9$, $c_s = \sqrt{2}/9$ and $(f^l)^2 = (f_\eta^l)^2 + (f_{\eta'}^l)^2$, $(f^s)^2 = (f_\eta^s)^2 + (f_{\eta'}^s)^2$. The leptonic decay constants f_h^l and f_h^s, for $h = \eta, \eta'$, for the light and strange correlations Γ_h^l and Γ_h^s, respectively, can be obtained from Eq. (15) with $g = f = l, s$, and $\Gamma_h^f(P) = \Gamma_{\mathrm{Ps}}(P)$ ($f = l, s$).

B. Numerical results for the η and η' masses, leptonic decay constants, and two-photon decay widths

The model parameters for the rainbow-ladder part of the kernel, together with the current masses of the light and strange quarks, are fixed by pion and kaon static properties; see Table I. The remaining parameters to be fixed are ξ and θ and these define the non-Abelian contribution to the kernel. We fix these parameters from experimental values of the masses, decay constants, and decay widths of the η and η', using a least-squares procedure. The experimental values of these constants are given in Table II.

We now fix ξ and θ by minimizing the root-mean-square fractional error for the η and η' masses and decay widths. The results for the parameters found in this way are given in the second row of Table III, and the corresponding values for the η and η' masses and decay widths are given in the first row of Table IV. As can be seen, the results are in

TABLE II. Experimental values for the masses, decay widths, and leptonic decay constants for η and η' mesons. All quantities are in MeV, except the decay widths which are in keV.

	m_η	$m_{\eta'}$	$\Gamma_{\eta\gamma\gamma}$	$\Gamma_{\eta'\gamma\gamma}$
PDG [48].	548	958	0.516(22)	4.35(36)

TABLE III. Parameters for the non-Abelian anomaly contribution the kernel. Λ_{UV} is given in MeV.

	ξ	$\cos^2\theta$	Λ_{UV}
CI model (fit-I)	8.15	0.898	823
CI model (fit-II)	5.54	0.999	810

TABLE IV. Masses and decay widths for η and η' mesons. All quantities are in GeV, except the decay widths are in keV.

	m_η	$m_{\eta'}$	$\Gamma_{\eta\gamma\gamma}$	$\Gamma_{\eta'\gamma\gamma}$
PDG [48]	548	958	0.516(22)	4.35(36)
CI model (fit-I)	548	920	0.287	4.62
CI model (fit-II)	558	920	0.418	4.16
Ding [49]	560	960	0.420	4.66
Osipov [55]	547	930	0.523	5.22
Takizawa [56]	510	$\cdots$	0.503*	$\cdots$

excellent agreement with experimental data, except for the decay width of the η meson, but we can do better as we now explain.

The UV cutoff parameter, Λ_{UV}, was introduced in Eq. (7) to regularize the divergent integrals appearing in the quark SDE and meson BSE. Together with α_{IR}, these parameters specify the RL contact interaction model. Recall that these parameters were determined using pion and kaon static properties. Similar, divergent integrals to Eq. (6) also appear in the non-Abelian part of the kernel, see Eqs. (21) and (22). Thus, in order to have a better description of the masses *and* decay widths for the η and η' mesons, we introduce another ultraviolet cutoff $\tilde{\Lambda}_{\mathrm{UV}}$ into the divergent integrals that appear in the non-Abelian part of the kernel in Eqs. (21) and (22), and fix ξ, θ, and $\tilde{\Lambda}_{\mathrm{UV}}$ by minimizing the root-mean-square fractional error for the η and η' masses and decay widths. This does not affect the results obtained for the pion and kaon. The reason for doing this is that the decay constants, and thus the decay widths, are sensitive to the ultraviolet cutoff used in the proper time regularization The results for the parameters, found in this way, are given in the second row of Table III, and the corresponding values for the η and η' masses and decay widths are given in the third row of Table IV. Clearly, our results agree nicely with experimental data for all four observables. In Table IV, we also list the results obtained in other approaches. The corresponding leptonic decay constants are given in Table V and also are in really good agreement with experimental data.

With all the parameters fixed, we now proceed to compute the transition form factors for the η and η' mesons.

TABLE V. Leptonic decay constants for the η and η' mesons. All quantities are in GeV.

	f_η^l	f_η^s	$f_{\eta'}^l$	$f_{\eta'}^s$
PDG [48]	0.090(13)	−0.093(28)	0.073(14)	0.094(8)
CI model (fit-I)	0.074	−0.060	0.078	0.086
CI model (fit-II)	0.081	−0.049	0.073	0.097
Ding [49]	0.074	−0.094	0.068	0.101

IV. TRANSITION FORM FACTORS FOR THE η AND η' MESONS IN A CONTACT INTERACTION

The transition process $\gamma^*\gamma \to h$ ($h = \eta, \eta'$) is characterized by a single transition form factor $G_h(Q^2)$, where Q^2 is the photon virtuality. For each meson, the transition form factor can be computed from, in a rainbow-ladder truncation, by [49]

$$
\begin{aligned}
&\frac{\alpha_{\mathrm{em}}}{2\pi}\epsilon_{\mu\nu\alpha\beta}q_{1\alpha}q_{2\beta}G_h(q_1^2, q_1\cdot q_2, q_2^2) \\
&= \frac{\alpha_{\mathrm{em}}}{2\pi}\epsilon_{\mu\nu\alpha\beta}q_{1\alpha}q_{2\beta}[G_h^l(Q^2) + G_h^s(Q^2)] \\
&= \mathrm{Tr}_D \int \frac{\mathrm{d}^4 q}{(2\pi)^4}[ic_l\chi_\mu^l(k, k_1)\Gamma_h^l(k_1, k_2)S_l(k_2)i\Gamma_\nu^l(k_2, k) \\
&\quad + ic_s\chi_\mu^s(k, k_1)\Gamma_M^s(k_1, k_2)S_s(k_2)i\Gamma_\nu^s(k_2, k)],
\end{aligned}
\tag{29}
$$

where the trace is over Dirac indices; the momentum distribution is $k_1 = k + q_1$ and $k_2 = q - q_2$; and the kinematic conditions are $q_1^2 = Q^2$, $q_2^2 = 0$, and $2q_1 \cdot q_2 = -(Q^2 + m_h^2)$ ($h = \eta, \eta'$). $\chi_\mu^f(k, p) = S_f(k)i\Gamma_\nu^f(k, p)S_f(p)$ ($f = l, s$) is the unamputated quark-photon vertex, and Γ_ν^f the (amputated) quark-photon vertex. In Eq. (29), all quantities have been determined earlier, namely we have already determined the model parameters and the masses of the η and η' mesons. Furthermore, we have obtained previously all quark propagators and Bethe-Salpeter amplitudes by solving their respective integral equations. Although the quark-photon vertex has been obtained in previous work, see for example, Ref. [16], we discuss it briefly for completeness.

A. The quark-photon vertex

The coupling of a photon with the bound state's charged constituent is given by the quark-photon vertex $\Gamma_\nu^f(p, k; Q)$, where f denotes the flavor of the quark that interacts with the photon, p (k) is the incoming (outgoing) quark momentum, and $Q = p - k$ is the photon momentum. The quark-photon vertex satisfies its own SDE but it is also constrained by the gauge invariance of quantum electrodynamics through the Ward-Takahashi identity

$$
iQ_\mu\Gamma_\mu(k, p; Q) = S^{-1}(k) - S^{-1}(p).
\tag{30}
$$

Satisfying this identity, and its $Q \to 0$ limit, is crucial for the conservation of the electromagnetic current [16].

In the RL truncation with a contact interaction, the SDE for the quark-photon vertex is [16]

$$
\Gamma_\mu(Q) = \gamma_\mu - \frac{4}{3}\alpha_{\mathrm{eff}}\int \frac{\mathrm{d}^4 q}{(2\pi)^4}\gamma_\nu S(q + Q)\Gamma_\mu(Q)S(q)\gamma_\nu.
\tag{31}
$$

Note that the RL truncation together with the contact interaction gives a quark-photon vertex that is independent of the relative momenta between the quark and the antiquark, and thus Γ_μ depends only on the photon momenta Q [16]. Therefore, the quark-photon vertex is given by

$$\Gamma_\mu(Q) = \gamma_\mu^T P_T(Q^2) + \gamma_\mu^L P_L(Q^2), \qquad (32)$$

where $Q_\mu \Gamma_\mu^T = 0$, and $\gamma_\mu^T + \gamma_\mu^L = \gamma_\mu$. The functions $P_T(Q^2)$ and $P_L(Q^2)$ can be found from Eq. (31) using standard projection methods; see Ref. [16] for details. It is found that $P_L = 1$ and

$$P_T(Q^2) = \frac{1}{1 - K_V(Q^2)}, \qquad (33)$$

where $K_V(Q^2)$ is the Bethe-Salpeter bound state kernel in the vector channel within the RL truncation of the SDE-BSE; see Eqs. (A10)–(A13) in Ref. [15]. Thus, because of the dressing of the quark-photon vertex, electromagnetic elastic and transition form factors will have a pole at $Q^2 = -m_V^2$, where m_V is the mass of the vector meson. In the RL truncation, the lowest masses are that of the ρ and ϕ vector mesons.

B. Numerical results for $G_h(Q^2)$ ($h = \eta, \eta'$)

In Fig. 1 we present our contact interaction results for the $\gamma^*\gamma \to \eta$ and $\gamma^*\gamma \to \eta'$ transition form factors, $G_\eta(Q^2)$ and $G_{\eta'}(Q^2)$, respectively, as a function of the photon virtuality Q^2, up to 20 GeV^2. In each case, we preset two curves, one
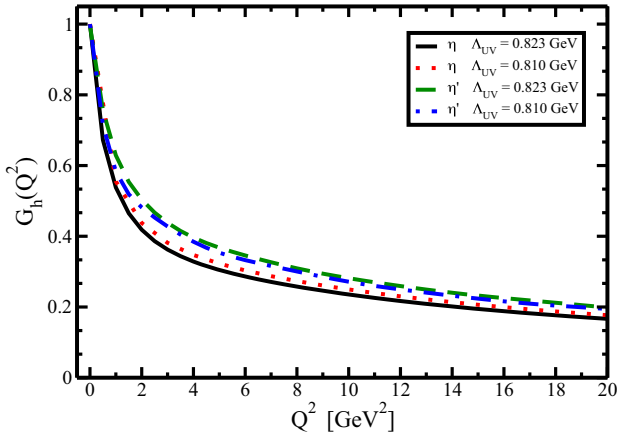

FIG. 1. Contact interaction results for transition form factors G_η and $G_{\eta'}$, normalized to one at $Q^2 = 0$, for two values of the ultraviolet cutoff in the divergent integrals of the non-Abelian part of the kernel. Solid and dashed curves (color: black and red) correspond to η and η' transition form factors with $\Lambda_{\mathrm{UV}} = 0.823$ GeV, respectively, and dotted and dot-dash curves (color: green and blue) to the transition form factor with $\Lambda_{\mathrm{UV}} \to \tilde{\Lambda}_{\mathrm{UV}} = 0.810$ GeV, respectively.

where we use the same cutoff Λ_{UV} as in the RL contribution to the kernel and one where we modify it to be $\tilde{\Lambda}_{\mathrm{UV}}$; see Table III. In the case of the static properties, changing Λ_{UV} in the non-Abelian part of the kernel, gives a better description of masses and decay constants. However, as can be seen, in the case of the transition form factor these two values give nearly equal results for both mesons.

From Fig. 1 we can see that both $G_\eta(Q^2)$ and $G_{\eta'}(Q^2)$ decrease as functions of Q^2, decreasing rapidly for small values of Q^2. However, for larger values of Q^2 (> 4 GeV^2), this decreasing is slower for both $G_\eta(Q^2)$ and $G_{\eta'}(Q^2)$. In Fig. 2, we plot $Q^2 G_\eta$ and $Q^2 G_{\eta'}$, for $\Lambda_{\mathrm{UV}} = 0.810$ GeV in the divergent integrals of the non-Abelian part of the kernel. From Figs. 1 and 2 we can see that both $G_\eta(Q^2)$ and $G_{\eta'}(Q^2)$ decrease slower than Q^2, in disagreement with perturbative QCD, which predicts that for very large Q^2 the product $Q^2 G_h(Q^2)$ becomes a constant [57–59]. This is not surprising for a contact interaction model, as we explain below. Finally, in Fig. 3 we compare our contact interaction results for G_η (top panel) and $G_{\eta'}$ (bottom panel), with $\Lambda_{\mathrm{UV}} = 0.810$ GeV, to the experimental results from CELLO [60], CLEO [61], and *BABAR* [62] Collaborations. We note that the data has been normalized to one at $Q^2 = 0$. For this we need the transition form factors at $Q^2 = 0$. This can be extracted from the experimental values for the decay widths, using $\Gamma_{h \to \gamma\gamma} = (1/4)\pi\alpha_{\mathrm{em}} m_h^3 |G_h(Q^2 = 0)|^2$ to obtain $G_\eta(0) = 0.2736$ and $G_{\eta'}(0) = 0.3412$ [48].

Clearly, while capable of describing η and η' static properties, a contact interaction framework markedly disagrees with experimental data for Q^2 greater than 2 GeV^2, and produces transition form factors in conflict with perturbative QCD. This is not surprising since the contact interaction produces a momentum independent dressed-quark mass function [7–31] and also Bethe-Salpeter equation kernels that are independent of the relative momentum
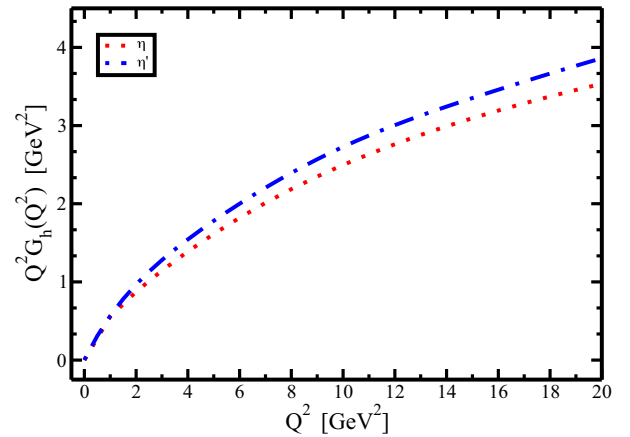

FIG. 2. Contact interaction results for $Q^2 G_\eta$ and $Q^2 G_{\eta'}$, for $\Lambda_{\mathrm{UV}} = 0.810$ GeV in in the divergent integrals of the non-Abelian part of the kernel.
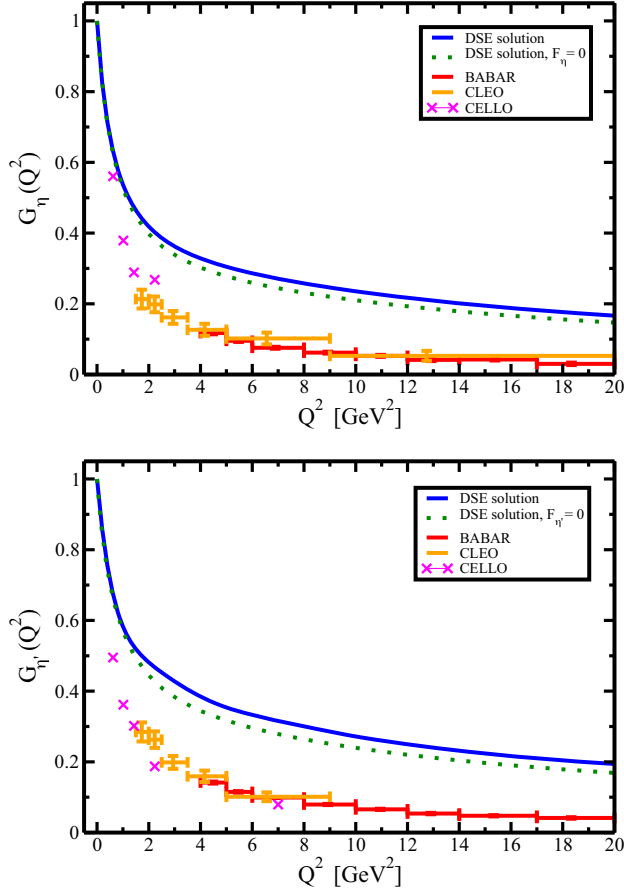
FIG. 3.   Contact interaction results for G_η (top panel) and $Q^2 G_{\eta'}$ (bottom panel), for $\Lambda_{\mathrm{UV}} = 0.810$ GeV, compared to experimental results from *BABAR*, CLEO, and CELLO.

between the quark and the antiquark [7–31], in contrast to QCD-based SDE studies and lattice QCD, These two features are fundamentally the source of the discrepancy between the elastic and transition form factor obtained with a contact interaction and those provided by experiment. However, our work highlights, and complements others [8,9,15,16,21,26], that elastic and transition form factor observables are very sensitive to the running (with momentum) of the dressed-quark mass; see Ref. [31] for a comparison of predictions for the nucleon and Δ elastic and transition form factors, made using interaction kernels that possess QCD-like momentum dependence with results obtained using a symmetry-preserving treatment of a vector $\times$ vector contact interaction.

Reference [31] makes clear that experiments are sensitive to the momentum dependence of the running couplings

and masses in QCD and highlights that in describing hadron properties it is crucial that a veracious expression of dynamical chiral symmetry breaking be incorporated in the bound-state problem. A momentum dependent gluon propagator, such as the one produced by lattice QCD simulations [63] or phenomenological studies of QCD's SDEs, consistent with QCD's gauge sector [37–40,64–69], will produce a momentum dependent dressed-quark mass function and Bethe-Salpeter amplitudes that are dependent of the relative momentum between the quark and the antiquark and therefore, for example, elastic and transition form factor of hadrons whose Q^2 dependence is in better agreement with experiment and perturbative QCD [31]. However, such improvement in the gluon propagator necessarily needs to be accompanied by a Bethe-Salpeter kernel that incorporates the non-Abelian anomaly. Only in this way can a proper description of the η and η' mesons be given [49].

V. SUMMARY AND CONCLUSIONS

We have constructed a contact interaction model for the η and η' mesons in a SDE-BSE approach to QCD and computed masses, decay widths and transition form factors. Tables IV and V show that this model gives an excellent description of the η and η' static properties, namely, their masses, decay width, and decay constants. Although contact interaction results for the η and η' transition form factors markedly disagree with experimental data for Q^2 greater than 2 GeV^2, and produces transition form factors in conflict with perturbative QCD, the fact that this model gives a very good description of the η and η' static properties makes it an excellent tool for the investigation of $U_A(1)$ symmetry restoration at finite temperature and density in the SDE-BSE approach to QCD. Work on this direction is under way and will be reported elsewhere.

[1] C. D. Roberts, EPJ Web Conf. **282,** 01006 (2023).

[2] C. D. Roberts, arXiv:2304.00154.

[3] C. D. Roberts and A. G. Williams, Prog. Part. Nucl. Phys. **33,** 477 (1994).

[4] P. Maris and C. D. Roberts, Int. J. Mod. Phys. E **12,** 297 (2003).

[5] A. Bashir, L. Chang, I. C. Cloet, B. El-Bennich, Y. X. Liu, C. D. Roberts, and P. C. Tandy, Commun. Theor. Phys. **58,** 79 (2012).

[6] C. S. Fischer, Prog. Part. Nucl. Phys. **105,** 1 (2019).

[7] L. X. Gutierrez-Guerrero, A. Bashir, I. C. Cloet, and C. D. Roberts, Phys. Rev. C **81,** 065202 (2010).

[8] H. L. L. Roberts, C. D. Roberts, A. Bashir, L. X. Gutierrez-Guerrero, and P. C. Tandy, Phys. Rev. C **82,** 065202 (2010).

[9] H. L. L. Roberts, A. Bashir, L. X. Gutierrez-Guerrero, C. D. Roberts, and D. J. Wilson, Phys. Rev. C **83,** 065206 (2011).

[10] H. L. L. Roberts, L. Chang, I. C. Cloet, and C. D. Roberts, Few-Body Syst. **51,** 1 (2011).

[11] C. Chen, L. Chang, C. D. Roberts, S. Wan, and D. J. Wilson, Few-Body Syst. **53,** 293 (2012).

[12] C. Chen, L. Chang, C. D. Roberts, S. M. Schmidt, S. Wan, and D. J. Wilson, Phys. Rev. C **87,** 045207 (2013).

[13] J. Segovia, C. Chen, I. C. Cloët, C. D. Roberts, S. M. Schmidt, and S. Wan, Few-Body Syst. **55,** 1 (2014).

[14] S. S. Xu, C. Chen, I. C. Cloet, C. D. Roberts, J. Segovia, and H. S. Zong, Phys. Rev. D **92,** 114034 (2015).

[15] M. A. Bedolla, J. J. Cobos-Martínez, and A. Bashir, Phys. Rev. D **92,** 054031 (2015).

[16] M. A. Bedolla, K. Raya, J. J. Cobos-Martínez, and A. Bashir, Phys. Rev. D **93,** 094025 (2016).

[17] K. Raya, M. A. Bedolla, J. J. Cobos-Martínez, and A. Bashir, Few-Body Syst. **59,** 133 (2018).

[18] F. E. Serna, M. A. Brito, and G. Krein, AIP Conf. Proc. **1701,** 100018 (2016).

[19] F. E. Serna, B. El-Bennich, and G. Krein, Phys. Rev. D **96,** 014013 (2017).

[20] Y. Lu, C. Chen, C. D. Roberts, J. Segovia, S. S. Xu, and H. S. Zong, Phys. Rev. C **96,** 015208 (2017).

[21] L. X. Gutiérrez-Guerrero, A. Bashir, M. A. Bedolla, and E. Santopinto, Phys. Rev. D **100,** 114032 (2019).

[22] J. L. Zhang, Z. F. Cui, J. Ping, and C. D. Roberts, Eur. Phys. J. C **81,** 6 (2021).

[23] L. X. Gutiérrez-Guerrero, G. Paredes-Torres, and A. Bashir, Phys. Rev. D **104,** 094013 (2021).

[24] Z. Xing, K. Raya, and L. Chang, Phys. Rev. D **104,** 054038 (2021).

[25] P. Cheng, F. E. Serna, Z. Q. Yao, C. Chen, Z. F. Cui, and C. D. Roberts, Phys. Rev. D **106,** 054031 (2022).

[26] X. Wang, Z. Xing, J. Kang, K. Raya, and L. Chang, Phys. Rev. D **106,** 054016 (2022).

[27] R. J. Hernández-Pinto, L. X. Gutiérrez-Guerrero, A. Bashir, M. A. Bedolla, and I. M. Higuera-Angulo, Phys. Rev. D **107,** 054002 (2023).

[28] Z. Xing and L. Chang, Phys. Rev. D **107,** 014019 (2023).

[29] Z. Xing, M. Ding, K. Raya, and L. Chang, arXiv:2301.02958.

[30] Z. Xing, M. Ding, and L. Chang, Phys. Rev. D **107,** L031502 (2023).

[31] J. Segovia, I. C. Cloet, C. D. Roberts, and S. M. Schmidt, Few-Body Syst. **55,** 1185 (2014).

[32] A. Ahmad, A. Bashir, M. A. Bedolla, and J. J. Cobos-Martínez, J. Phys. G **48,** 075002 (2021).

[33] F. E. Serna and G. Krein, EPJ Web Conf. **137,** 13015 (2017).

[34] K. l. Wang, Y. x. Liu, L. Chang, C. D. Roberts, and S. M. Schmidt, Phys. Rev. D **87,** 074038 (2013).

[35] D. Dudal, J. A. Gracey, S. P. Sorella, N. Vandersickel, and H. Verschelde, Phys. Rev. D **78,** 065047 (2008).

[36] M. Q. Huber, R. Alkofer, and S. P. Sorella, AIP Conf. Proc. **1343,** 158 (2011).

[37] P. O. Bowman, U. M. Heller, D. B. Leinweber, M. B. Parappilly, and A. G. Williams, Phys. Rev. D **70,** 034509 (2004).

[38] P. Boucaud, J. P. Leroy, A. L. Yaouanc, J. Micheli, O. Pene, and J. Rodriguez-Quintero, Few-Body Syst. **53,** 387 (2012).

[39] A. Ayala, A. Bashir, D. Binosi, M. Cristoforetti, and J. Rodriguez-Quintero, Phys. Rev. D **86,** 074512 (2012).

[40] F. Gao, S. X. Qin, C. D. Roberts, and J. Rodriguez-Quintero, Phys. Rev. D **97,** 034010 (2018).

[41] D. Ebert, T. Feldmann, and H. Reinhardt, Phys. Lett. B **388,** 154 (1996).

[42] Y. Nambu, Prog. Theor. Phys. **5,** 614 (1950).

[43] E. E. Salpeter and H. A. Bethe, Phys. Rev. **84,** 1232 (1951).

[44] M. Gell-Mann and F. Low, Phys. Rev. **84,** 350 (1951).

[45] N. Nakanishi, Prog. Theor. Phys. Suppl. **43,** 1 (1969).

[46] P. Maris, C. D. Roberts, and P. C. Tandy, Phys. Lett. B **420,** 267 (1998).

[47] P. T. P. Hutauruk, J. J. Cobos-Martínez, Y. Oh, and K. Tsushima, Phys. Rev. D **100,** 094011 (2019).

[48] R. L. Workman *et al.* (Particle Data Group), Prog. Theor. Exp. Phys. **2022,** 083C01 (2022).

[49] M. Ding, K. Raya, A. Bashir, D. Binosi, L. Chang, M. Chen, and C. D. Roberts, Phys. Rev. D **99,** 014014 (2019).

[50] T. Feldmann, P. Kroll, and B. Stech, Phys. Lett. B **449,** 339 (1999).

[51] T. Feldmann, P. Kroll, and B. Stech, Phys. Rev. D **58,** 114006 (1998).

[52] T. Feldmann, Int. J. Mod. Phys. A **15,** 159 (2000).

[53] N. Nakanishi, Phys. Rev. **138,** B1182 (1965).

[54] N. Nakanishi, Phys. Rev. **139,** B1401 (1965).

[55] A. A. Osipov, B. Hiller, and A. H. Blin, Acta Phys. Pol. B Proc. Suppl. **8,** 183 (2015).

[56] M. Takizawa, Y. Nemoto, and M. Oka, Aust. J. Phys. **50,** 187 (1997).

[57] G. P. Lepage and S. J. Brodsky, Phys. Rev. D **22,** 2157 (1980).

[58] G. P. Lepage and S. J. Brodsky, Phys. Lett. **87B,** 359 (1979).

[59] A. V. Efremov and A. V. Radyushkin, Phys. Lett. **94B,** 245 (1980).

[60] H. J. Behrend *et al.* (CELLO Collaboration), Z. Phys. C **49,** 401 (1991).

[61] J. Gronberg *et al.* (CLEO Collaboration), Phys. Rev. D **57,** 33 (1998).

[62] P. del Amo Sanchez *et al.* (*BABAR* Collaboration), Phys. Rev. D **84,** 052001 (2011).

[63] D. Dudal, O. Oliveira, and P. J. Silva, Ann. Phys. (Amsterdam) **397,** 351 (2018).

[64] D. Binosi, L. Chang, J. Papavassiliou, and C. D. Roberts, Phys. Lett. B **742**, 183 (2015).

[65] P. Boucaud, T. Bruntjen, J. P. Leroy, A. Le Yaouanc, A. Y. Lokhov, J. Micheli, O. Pene, and J. Rodriguez-Quintero, J. High Energy Phys. 06 (2006) 001.

[66] A. C. Aguilar, D. Binosi, and J. Papavassiliou, Phys. Rev. D **86**, 014032 (2012).

[67] D. Binosi, L. Chang, J. Papavassiliou, S. X. Qin, and C. D. Roberts, Phys. Rev. D **95**, 031501 (2017).

[68] D. Binosi, C. D. Roberts, and J. Rodriguez-Quintero, Phys. Rev. D **95**, 114009 (2017).

[69] D. Binosi, C. Mezrag, J. Papavassiliou, C. D. Roberts, and J. Rodriguez-Quintero, Phys. Rev. D **96**, 054026 (2017).